Chapter

Aggregation of Partially Hydrophilic Silica Nanoparticles in Porous Media: Quantitative and Qualitative Analysis

Siti Rohaida Mohd Shafian, Ismail M. Saaid, Norzafirah Razali, Ahmad Fadhil Jahari and Sonny Irawan

Abstract

In this experimental work, the adsorption of partially hydrophilic silica nanoparticles, SiO_2 has been investigated to determine the degree of silica nanoparticle aggregation in the porous media. An integrated quantitative and qualitative method was used by flowing silica nanoparticles into Buff Berea cores and glass micromodel. Water wet Buff Berea cores were flooded with 5 pore volumes of 0.05% silica nanoparticles solution followed by 10 pore volumes of brine post flush subjected to 30 and 60°C. The pressure drops increased rapidly at the initial stage of silica nanoparticles injection indicated the adsorption had taken place. Pressure drops reached the maximum value of ~3.1 psi and between 26.6–82.6 psi at 30 and 60°C respectively. Pressure drops gradually declined and stabilized in between ~0.4 and ~0.7 psi after couple of pore volumes of brine post flush, suggesting complete reversible and irreversible adsorption. Micromodel test provide qualitative information where the straining or log-jamming observed in the form of gelled-like suspension when silica nanoparticles in contact with brine. The adsorption is considered reversible when the suspension decreased after post flooded with brine. Silica nanoparticles used in this experimental work shows minimal aggregation that can be beneficial as improved oil recovery agent.

Keywords: nanotechnology, nanoparticles, silica nanoparticles, aggregation, adsorption, porous media, core flooding, micromodels, permeability impairment

1. Introduction

The advancement of nanotechnology attract researchers interest for its application in oil and gas that include the application for enhanced oil recovery, exploration, drilling, completion, well logging, chemical stabilizer, conformance control, heavy oil, stimulation and fines migration control [1–13]. The unique properties of nanoparticles comprises of extremely high surface area compared to their small sizes, thermally stable, high potential to alter the wettability of the reservoir formations, modify rock surface charges and associated impact on the rheological properties of suspensions [14] that showed potentials to enhance extraction of

hydrocarbons. Silica nanoparticles, SiO_2 for example, can be found in most non-toxic inorganic materials which also the main component of sandstone rock, and is more environmental friendly compared to chemical based materials. Nanoparticles have showed remarkable performance in fixing the formation fines during fracturing activities [12]. Several studies suggested the nanoparticles has the effect of strengthening the attractive forces with regards to the repulsive forces and prevent the detachment of fines particles from the pore walls [15].

Nanoparticles are very small in nature with size range between 1 and 100 nm [16] which permits this tiny particles to flow in the porous media and show distinctive behavior which fascinating from petroleum engineering perspective. During nanoparticles transport in porous media, the physicochemical attraction between particles and the pore walls can lead to adsorption or retention that occurs as reversible and irreversible [17, 18]. Adsorption in porous media can create major issue and need to be control to avoid significant formation damage. Abdelfatah described; three different mechanisms were taken place when nanoparticles interact in the pores. These interactions are surfaces deposition, mono-particle plugging and multi-particles plugging [19]. The surface deposition interactions are dominated by five type of forces; the attractive potential force of Van der Waals, repulsion force of electric double layers, Born repulsion, acid–base interaction, and hydrodynamics [20]. The adsorption of nanoparticles and the pore walls will occur when the total force is negative, where the attraction is larger than repulsion between nanoparticles and pore walls.

The mono-particle plugging or screening or mechanical entrapment occur when larger particle block at the narrow pores. Injecting large volume of nanoparticles can lead to mono-particle plugging. Multi-particles plugging or log-jamming mechanism is similar to mono-particle plugging but the blocking occurs at pore channel larger than nanoparticles size. Log-jamming happen when nanoparticles flow from pores to narrow pore throat. Nanoparticles interaction between the particles itself can cause aggregation and gelation and the significantly block the pore throat if the aggregate size much bigger than pore throat. The adsorption of nanoparticle on the pore walls also depends on the type and pH of nanoparticles, rock clay content as well as the rock wettability [21]. The advantage of nanoparticles adsorption, instead, it contributed to the alteration of rock wettability that is desirable for

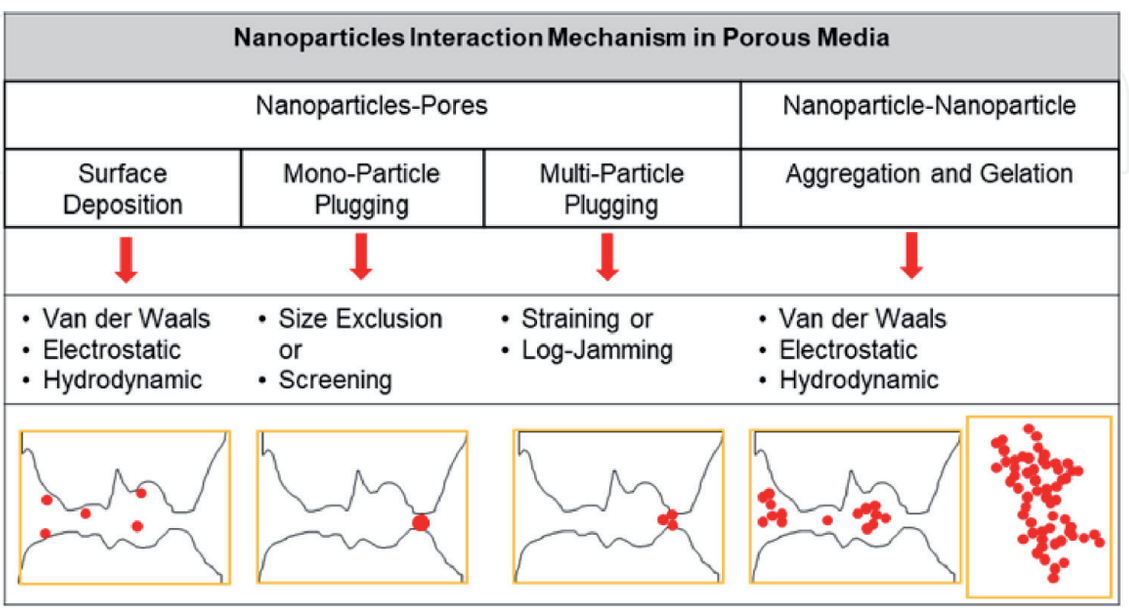

Figure 1.
Nanoparticles interactions mechanisms in porous media [19].

enhanced oil recovery [22–25]. Nanoparticles specifically silica nanoparticles on the other hand, are not stable in salts water and aggregates at elevated temperature, high concentration and at high injection rates that can lead to substantial permeability impairment [17, 24, 26–28]. **Figure 1** shows the illustration of nanoparticles interactions mechanisms in porous media.

This experimental work investigates the aggregation of partially hydrophilic silica nanoparticles, SiO_2 in porous media. The standard method for silica nanoparticles concentration measurement using UV-Vis spectrophotometer is not suitable, and hence more reliable quantitative and qualitative methods were developed. Core flooding pressure drops and particles size analysis of treated Buff Berea cores provide quantitative information supported by qualitative measurement of Field Emission Scanning Electron Microscope (FESEM) and micromodel test. The pressure drops value showed closed agreements with particles size during silica nanoparticles injection and brine post flush, visualization of silica nanoparticles in micromodel. FESEM analysis suggested the partially hydrophilic silica nanoparticles used in this experimental work showed minimal aggregation with insignificant permeability impairment.

2. Materials and methods

2.1 Materials for core flooding

2.1.1 Nanofluids

Partially hydrophilic silica nanoparticles (SiO_2) supplied by commercial nanomaterials company using code name NPN-ST. This nanoparticles was selected based the requirement of this research work in terms of size and solubility in water and selected solvent. NPN-ST supplied at 30% active concentration with average size of 12 nm and pH 5. NPN-ST was diluted in mutual solvent at 0.05% concentration and the solution undergoes sonication in ultrasonic bath for at least 40 minutes.

NPN-ST stability in the carrier fluid before and after 24 hours aged at room temperature and 60°C was determined through visual observation, turbidity test and particle size distribution measurement. The particle size of NPN-ST slightly increased from 24 nm to ~27 nm and 35 nm after kept for 24 hours at room temperature and at 60°C respectively. The incremental of particle size is minor which is within the accepted size required for this study.

The turbidity reading is in the low range between 0.95 and 1.98 NTU. **Figure 2** shows the particles size distribution and visual observation of NPN-ST after 24 hours sustained as clear solution and did not show any forms of precipitation. **Figure 3** shows the Transmission Electron Microscopy (TEM) image of NPN-ST solution at 20 and 100 nm scale which comparable with most common silica nanoparticles materials.

2.1.2 Fluid samples

Formation brine used in this study is mixture of major ion salts prepared in deionized water. $CaCl_2$, $MgCl_2$, KCl and NaCl salts were mixed in the appropriate proportions to make up 1.5 wt% formation water salinity. Brine sample was filtered with the Millipore vacuum filter through a 47 mm, 0.45 micron nominal pore opening cellulose filter. **Table 1** shows the brine composition of synthetic formation water.

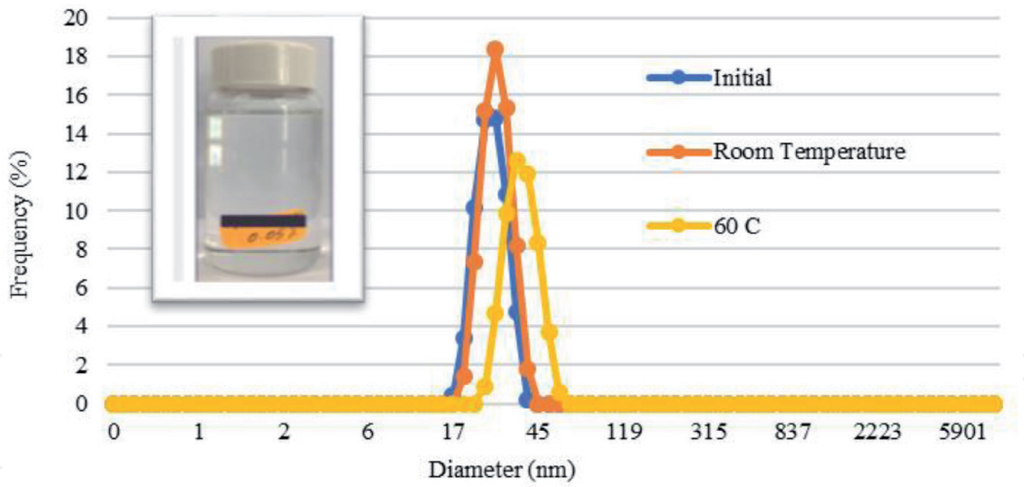

Figure 2.
Particle size and visual observation of NPN-ST at initial and after 24 hours aged at room temperature and 60°C.

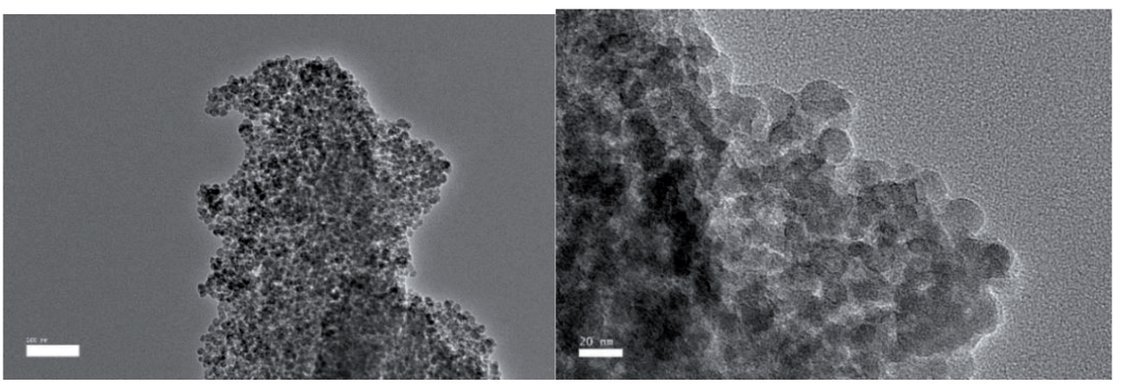

Figure 3.
Image of 0.05% NPN-ST under transmission electron microscopy (TEM): (a) at 100 nm scale and (b) at 20 nm scale.

Salts	Weight for 1 L (g)
NaCl	20.92
KCl	0.31
$MgCl_2.6H_2O$	0.08
$CaCl_2$	0.10

Table 1.
Salt composition for formation brine.

2.1.3 Core samples

Buff Berea cores of 3.8 cm in diameter and 7.5 cm in length (and 2 sets of core with 14.0 cm in length), permeability range between 200 and 400 mD that contained mixture of clays were used in this study. Five sets of core flood tests were conducted and details of core properties assigned for each experiment are listed in **Table 2**. **Table 3** shows the Buff Berea core detail mineralogy measured by X-Ray Diffraction (XRD) test.

Core ID	Diameter (cm)	Length (cm)	Porosity (%)	Air permeability (md)	Pore volumes (ml)	Test temperatures (°C)
B1–10	3.84	7.40	23.35	386.79	20.10	30
B3–21	3.84	7.44	23.20	328.89	20.02	30
L1	3.84	14.18	N.D.[1]	N.D.[1]	37.90	30
B7-16	3.84	7.44	23.50	325.42	19.82	60
L2	3.84	14.55	N.D.[1]	N.D.[1]	38.89	60

[1]*Not determine.*

Table 2.
Buff Berea core properties.

Core	Calculated whole rock composition (weight %)						
	Quartz	Plagioclase	K-Feldspar	Calcite	Dolomite	Siderite	Pyrite
Buff Berea	79.2	4.3	1.9	0.4	1.1	0.9	1.0
	Clay fraction Clay fraction (clay typing, weight %)						
	Kaolinite	Chlorite	Illite	Mixed layer (I/S)	Smectite	Total clay	
	36.2	19.7	33.2	7.9	2.5	10.7	

Table 3.
Buff Berea core X-ray diffraction (XRD) data.

2.2 Core flooding procedure

The dry weight of the core was measured before brine saturation. Core was saturated in desiccator with formation brine until all air trapped were removed. The core was then put in saturator for further saturation at 2000 psi for 24 hours. The saturated weight of the core was measured after saturation to calculate the core pore volume (PV) by gravimetric method. The core was carefully unloaded from saturator, into core holder and subject to 1500 psi confining pressure applied with mineral oil using automatic confining pressure pump. The back pressure was set at 200 psi and temperature set at 30 and 60°C. The core was flooded with brine for at least 2 pore volumes or until pressure stabilize at 0.5, 1.0 and 1.5 ml/min. The derived pressure drops data were used to calculate absolute permeability to water using Darcy's Law. The core flooding test was conducted using Formation Response Test (FRT) equipment model 3100. Core flooding equipment consists of:

- 12-inch core holder (1.5-inch diameter)
- Backpressure regulator
- 3 accumulators (1000 ml volume)
- A system of valves operated pneumatically via a computer
- An injection system, incorporating an electronically-controlled Quizix pump

- Automated auto sampler
- A balance to a data logger

Figure 4 shows the schematic of core flooding equipment.

After brine injection, 5 pore volumes of 0.05% SiO_2 NPN-ST was injected into Buff Berea core at 0.5 ml/min and aged for 24 hours. The core was flooded with brine for 10 pore volumes at 0.5 ml/min or until stable pressure drops is obtained. Finally, core is subjected to 2 pore volumes of brine at 0.5, 1.0 and 1.5 ml/min to determine the final permeability to water. The effluent during NPN-ST and brine post flush injection were collected every 5 ml per tube and analyzed for particle size using light scattering method. After completion of core flooding test, each of the treated Buff Berea cores were dried and cut into three sections (inlet, middle and outlet) for Field Scanning Electron Microscope (FESEM) analysis. The attachment and aggregation of silica nanoparticles under FESEM were determined by comparing the photomicrographs of untreated core (obtained from same core cut with treated cores).

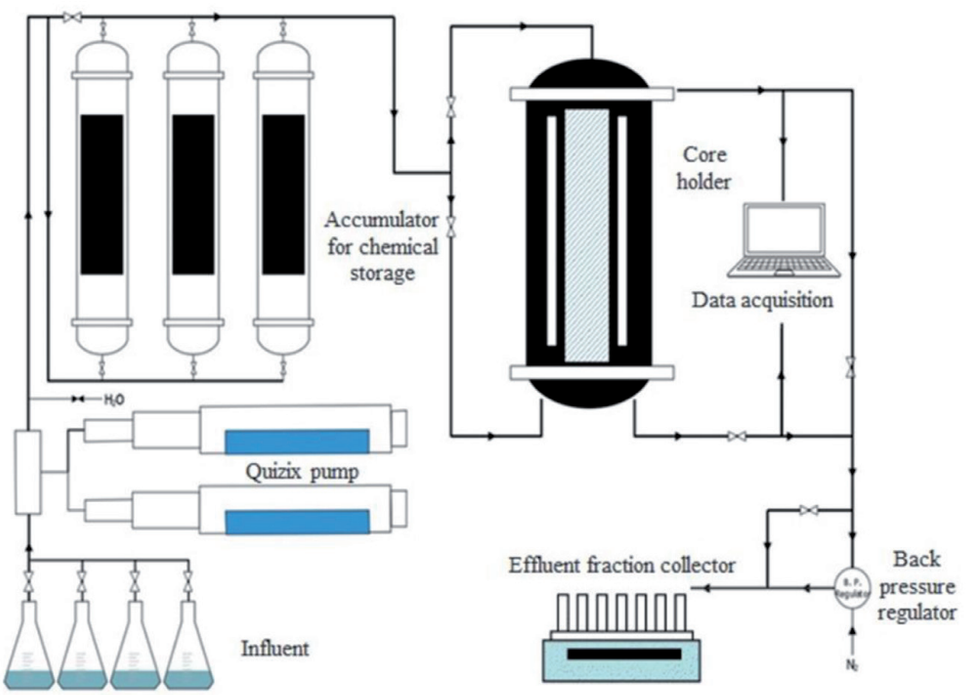

Figure 4.
Schematic of core flooding equipment.

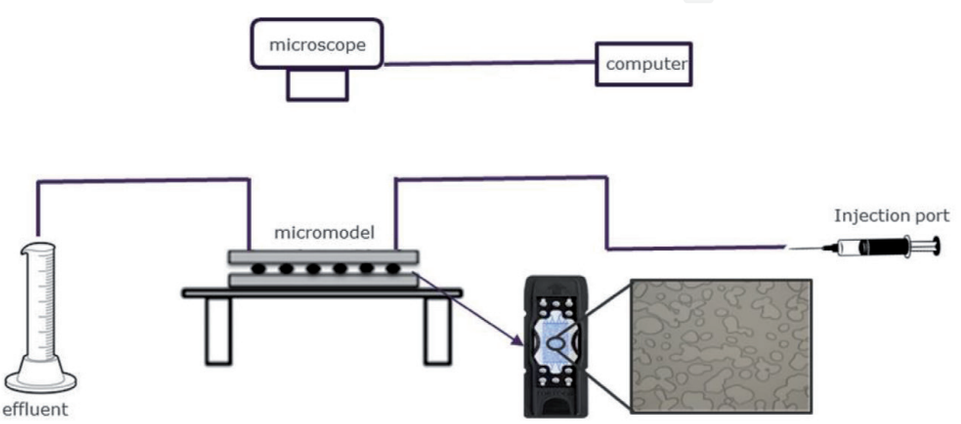

Figure 5.
Schematic of micromodel system.

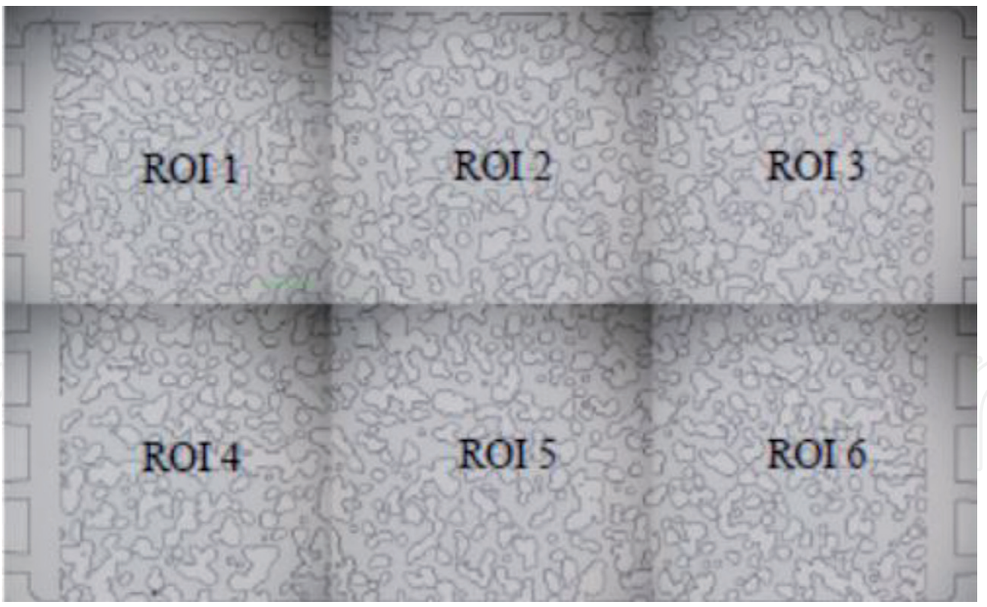

Figure 6.
Region of interest (ROI) at inlet, middle and outlet of the micromodel porous network.

Properties	Fine	Medium	Coarse
Pore size (μm)	36.33–87.76	90.3–191.4	205.37–441.46
Grain size (μm)	110.27–186.08	209.82–305.02	387.13–705.90

Table 4.
Micromodel pore and grain size.

2.3 Micromodel test

Figure 5 illustrates the micromodel experimental set up that comprised of 3 main components; the injection port and lines, that include the differential pressure set up (bypassed for this study), a flow cell represents as porous network (45 mm × 15 mm dimension) with 2.5 Darcy permeability that made of borosilicate glass and the slide made of polypropylene. The flow cell is placed under NIS-Element AR microscope which has 2X, 4X, 8X and 20X zoom lenses connected to a computer for image viewing. Six region of interest (ROI) have been identified at inlet, middle and outlet site of the micromodel. The images were taken by using microscope at 2X resolution.

Figure 6 shows the ROIs used for this micromodel experiment. The pore and grain size of micromodel is categorized as fine, medium and coarse. The pore and grain size output indicate the overall ROIs studies. **Table 4** shows the micromodel pore and grain size determined by using Annotations and Measurement tool on microscope software. 30 ml of 0.05% NPN-ST was injected at 0.001 ml/min followed by 40 ml of 1.5 wt% brine at 0.1 ml/min into the glass micromodel and aged for 1 week. After 1 week, 30 ml of brine was injected and the micromodel image of each ROI was analyzed.

3. Results and discussion

3.1 Core flooding test

For this study, 0.05% NPN-ST concentration was selected based on gravity-assisted flow (GAF) reported in previous work [29]. Injection rate was fixed at

0.5 ml/min throughout the injection to eliminate the permeability impairment caused by nanoparticles injection at high rates [27]. The recorded pressure drops during initial brine, NPN-ST and brine post flush injection enable the interpretation of silica nanoparticles adsorption or plugging inside the porous media. **Figure 7** shows the pressure drop profiles of water wet Buff Berea core; B1–10, B3–21 and L1 when injected with 0.05% NPN-ST at 30°C. B1–10 core flood results showed rapid increased in pressure drops from ~0.28 psi to maximum ~1.09 psi after 2.6 pore volumes of NPN-ST injection. The rapid increased of pressure drops at initial stage of silica nanoparticles injection caused by multilayer adsorption and gradual straining effects [17, 18]. After 2.6 pore volumes, the pressure drops gradually declined to ~0.87 psi that indicates the adsorption process had completed. The pressure drops start to increase rapidly to maximum ~1.16 psi during brine post flush which confirmed the NPN-ST multilayers adsorption. The pressure drops gradually declined after 2.4 pore volumes brine post flush and stabilized and reached steady state at 0.37 psi after six pore volumes that indicate no further detachment and straining of NPN-ST.

B3–21 and L1 core generated slightly higher pressure drops at initial stage and during post flush but with similar trend with B1–10 core. The pressure drops of L1 core increased rapidly from ~0.5 psi to maximum ~2.3 psi. After 1.56 pore volumes of NPN-ST injection, the pressure drops declined and stabilized at ~1.9 psi and further declined during brine post flush and stabilized at ~0.77 psi. Multilayer adsorption and gradual straining effects of B3–21 generated the highest pressure drops from ~0.27 to maximum 3.11 psi compared to B1–10 and L1 core. Nevertheless, B3–21 reached steady state at 0.4 psi, which slightly higher compared to B1–10 core. **Figure 8** shows the pressure drop profiles of Buff Berea core B7–16 and L2 when injected with 0.05% NPC-ST at 60°C. After brine injection, sharp increase in pressure drop from ~0.20–0.24 psi to maximum ~ 0.9–1.53 psi was observed. After 2.7 pore volumes of NPC-ST injection, the pressure drop temporary decline until sharp increase in pressure drop to maximum value of 82.61 and 26.61 psi for B7–16 and L2 core respectively. The maximum pressure drops observation occurred for less than 1 pore of NPN-ST injection until the pressure drop gradually declined and stabilized at ~ 0.28–0.30 psi. Pressure drop at 60°C showed more rapid increasing in pressure

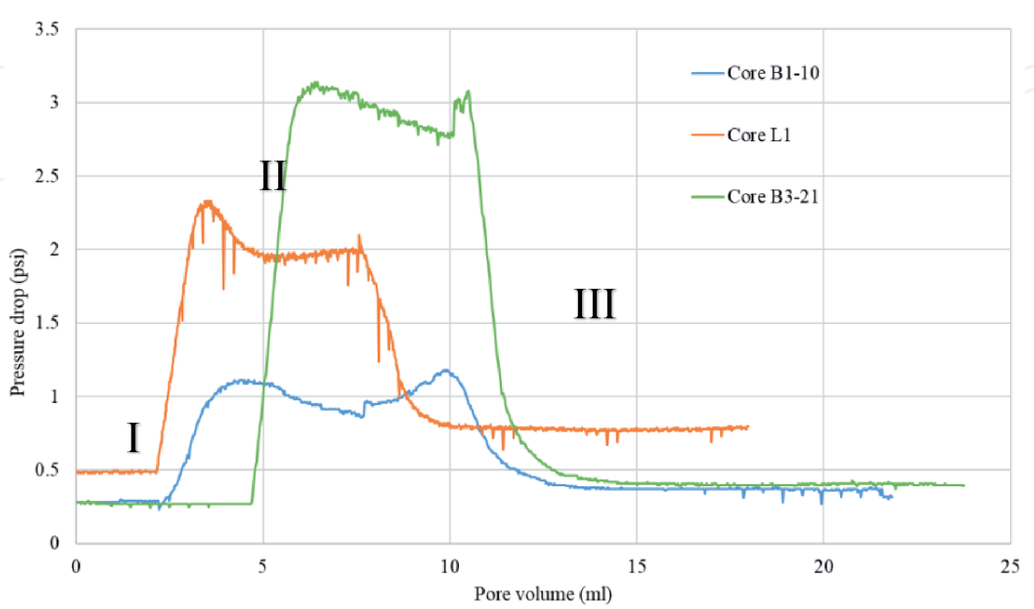

Figure 7.
Pressure drops of buff Berea Core B1–10, B3–21 and L1 during (I) initial brine injection, (II) 0.05% NPN-ST injection and (III) brine post flush at 30°C.

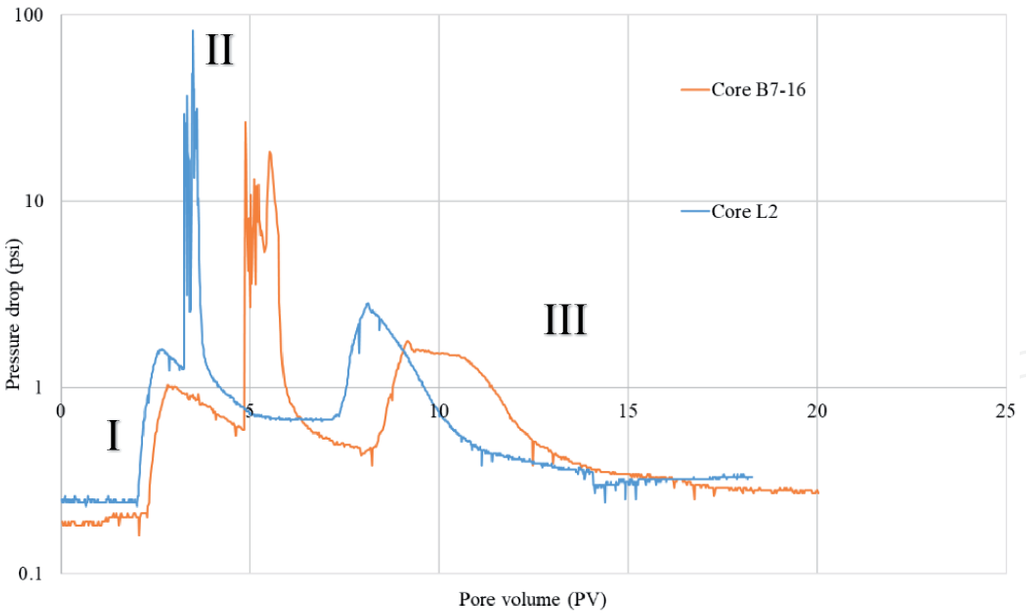

Figure 8.
Pressure drops of buff Berea Core B7–16 and L2 (I) initial brine injection, (II) 0.05% NPN-ST injection and (III) brine post flush at 60°C.

drops in comparison with 30°C during NPC-ST injection, but the permeability impairment is slightly lower at 60°C.

The permeability before and after silica nanoparticles injection were calculated using the pressure drops data during brine injection and calculated using Darcy's law.

$$k = \frac{Q\mu L}{A\Delta P} \tag{1}$$

where k (D), Q (cm^3/sec), μ (cP), L (cm), A (cm^2) and ΔP (atm) is permeability, flow rate, water viscosity, core length, core area and pressure drops respectively.

Table 4 shows the calculated permeability impairment of Buff Berea core B1–10, B3–21, L1, B7–16 and L2 after NPN-ST injection. The permeability impairment of each treated cores were calculated using the following equation:

$$Permeability\ impairment, k_{imp} = \left[\frac{(kw_i - kw_f)}{kw_i}\right] x\ 100\% \tag{2}$$

where k_{imp}, k_{wi} and k_{wf} is permeability impairment, initial permeability and final permeability respectively.

The calculated permeability impairment for B1–10, B3–21, L1, B7–16 and L2 are 28.6, 30.3 and 26.2% for 30°C and 19.6 and 16.4% at 60°C respectively as shown in **Table 5**. The permeability impairment between cores at designated temperature showed close values and slightly lower compared with other silica nanoparticles investigated in previous study [25–27]. Permeability impairment at 60°C is lower compared to 30°C indicated the silica nanoparticles used in this study is suitable for high temperature application.

3.2 Field scanning electron microscope (FESEM) analysis

FESEM photomicrographs of untreated core and cores injected with NPN-ST were compared to confirm the silica nanoparticles adsorption on core surface. At 500 nm magnification, untreated core displays as uniform surface as shown in **Figure 9**. Spherical shape of silica nanoparticles were detected on surface of B3–21

Core ID	Test temperature (°C)	Initial core permeability, k_{wi} (mD)	Final core permeability, k_{wf} (mD)	Permeability impairment, k_{imp} (%)
B1–10	30	247.8	176.8	28.6
B3–21	30	229.3	159.9	30.3
L1	30	234.8	173.3	26.2
B7–16	60	193.9	155.9	19.6
L2	60	253.5	211.9	16.4

Table 5.
Permeability impairment of buff Berea core B1–10, B3–21, L1, B7–16 and L2.

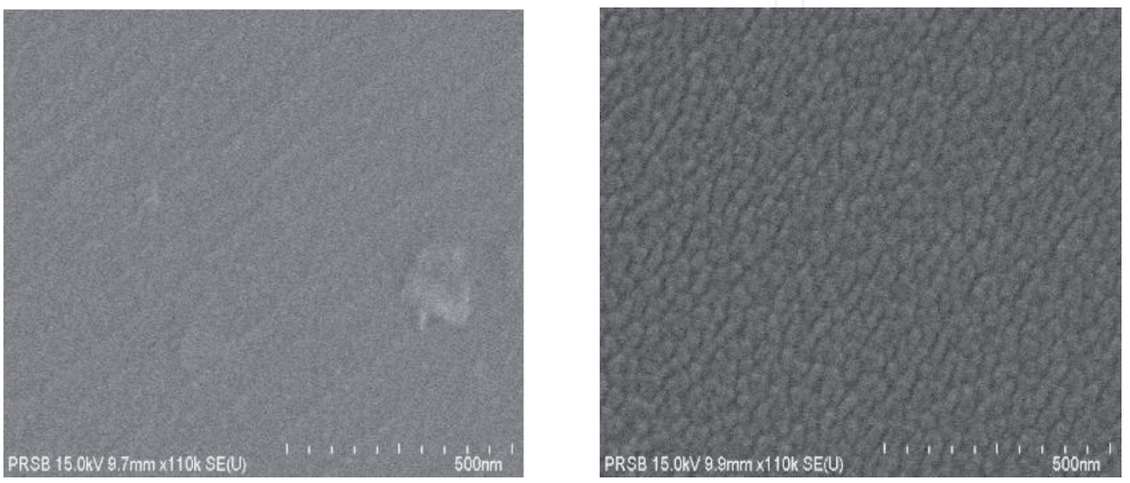

Figure 9.
FESEM photomicrographs of untreated buff Berea core at 500 nm magnification.

core with average particle size between 30 and 36 nm. Some aggregation of silica nanoparticles was observed at the inlet and middle core section and can be consider as minimal aggregation. Clear image of spherical silica nanoparticles adsorbed on the surface of L1 core observed at the inlet, middle and outlet section which also consider minimal aggregation. For both B1–10 and L1 core, most of the spherical particles was observed at the outlet section of the core where the non-adsorb silica nanoparticles was flushed out during post brine injection. **Figures 10** and **11** shows the FESEM photomicrographs at inlet, middle and outlet section of B1–10 and L1 core at 500 nm magnification.

On the other hand, no clear silica nanoparticles image detected for B7–16 and L2 core at inlet and middle section. Most of the spherical shape which also formed as aggregates observed at the outlet core section but the high charging during FESEM analysis caused unclear photomicrographs image as shown in **Figures 12** and **13**. Further analysis of aggregation of silica nanoparticles inside the porous media showed the aggregation could be substantial when in contact with residual water in the core. High aggregation can cause serious pore plugging and ultimately reduce the permeability. The silica nanoparticles spherical shape attached with each other and formed aggregates as shown in **Figure 14**.

3.3 Particle size of core flood effluents

The particles size of silica nanoparticles and post flush effluents provide indirect relationship with silica nanoparticles aggregation in the porous media. The

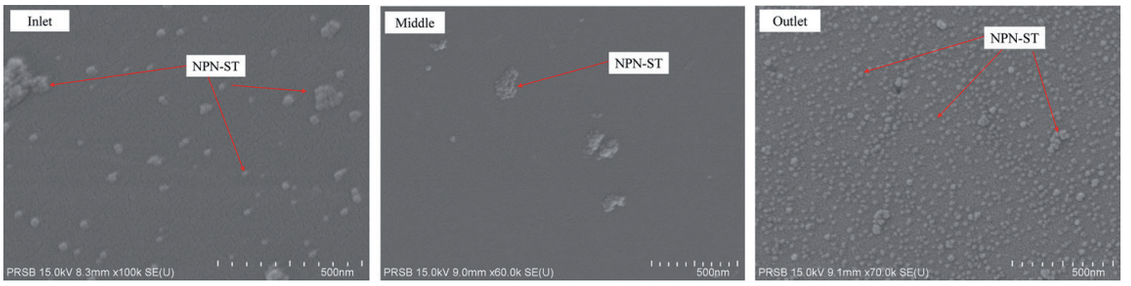

Figure 10.
FESEM photomicrographs of buff Berea core B1–10 treated with NPN-ST.

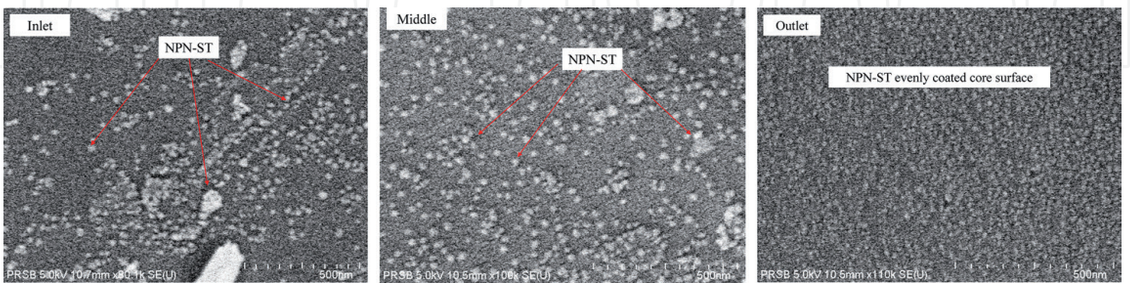

Figure 11.
FESEM photomicrographs of buff Berea core L1 treated with NPN-ST.

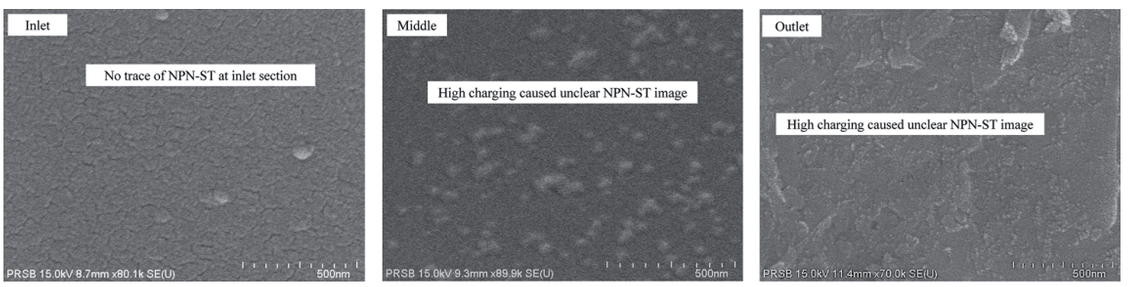

Figure 12.
FESEM photomicrographs of buff Berea core B7–16 treated with NPN-ST.

measured effluent particle size during NPN-ST is smaller compared to brine post flush as shown in blue line in **Figures 15–17**. Most of silica nanoparticles aggregates were flushed out, while the majority of larger particles size was detected during brine post flush as shown in orange line in **Figures 15–17**. The measurement of particles size provides useful information for this experimental work where the larger particles size corresponds with high pressure drops and vice-versa.

3.4 Micromodel test

The qualitative method using glass micromodel flooding test allow the in-situ visualization during silica nanoparticles injection and brine injection that enable the image capture for aggregation analysis. The micromodel porous network before fluid injection is shown **Figure 18**. Silica nanoparticles particles propagate in the porous media that captured at the respective ROIs marked in red circle as shown in **Figure 19**. Gelled liked suspension was observed in the porous network when the silica nanoparticles in contact with brine that indicate aggregation marked in red arrow as shown in **Figure 20**. The size of aggregation at respective ROIs was measured according to fine, medium and coarse.

The aggregation phenomena associated with the sharp increase in pressure drops observed during core flooding test when silica nanoparticles injected into water

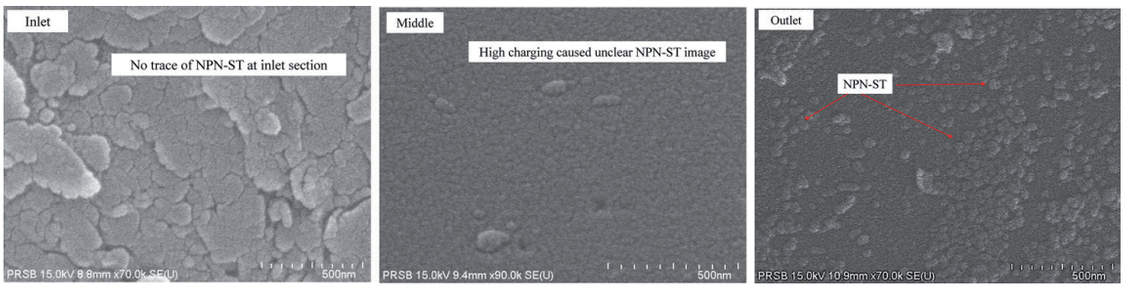

Figure 13.
FESEM photomicrographs of buff Berea core L2 treated with NPN-ST.

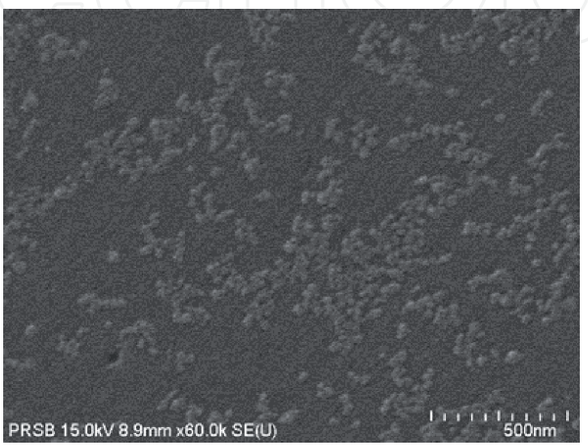

Figure 14.
FESEM photomicrographs of silica nanoparticles aggregation in the outlet section of buff Berea core.

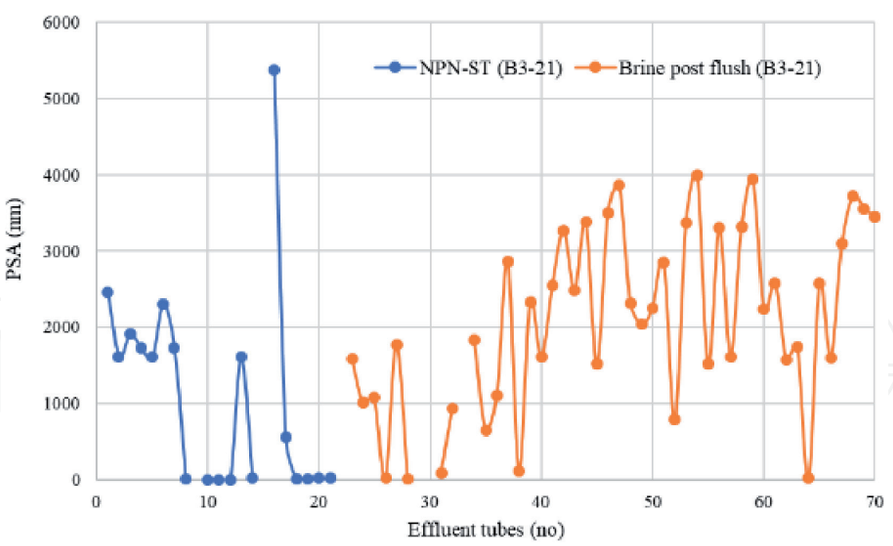

Figure 15.
B3–21 core effluent particles size during NPN-ST injection and brine post flush.

wet Buff Berea core. The treated micromodel was aged for 1 week to investigate the degree of aggregation. Post brine injection flushed out some of the silica nanoparticles suspension as shown in **Figure 21**. The size of aggregation size at respective ROIs was measured to compare with the initial stage of brine injection. The reduction of gelled-size aggregates results corresponds with the declined in pressure drops during brine post flush injection. Gel-liked suspension remains adsorbed in some parts of the porous network and strained on the pore walls. In relation, during

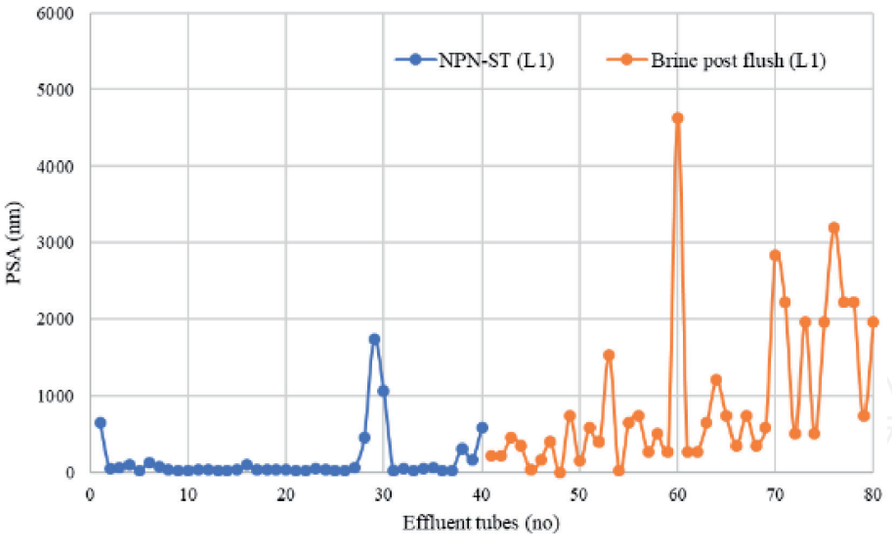

Figure 16.
L1 core effluent particles size during NPN-ST injection and brine post flush.

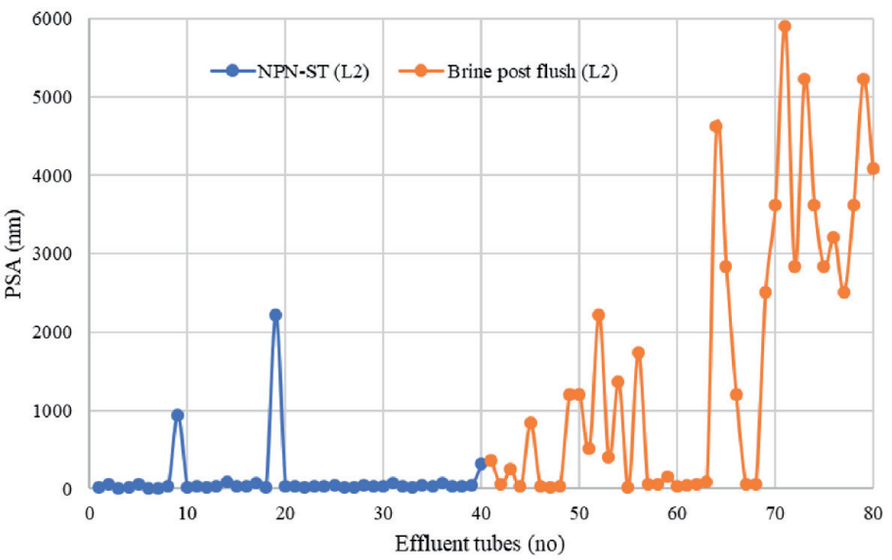

Figure 17.
L2 core effluent particles size during NPN-ST injection and brine post flush.

core flooding test, silica nanoparticles adsorption and straining will reduce the core permeability and block the fluid pathways.

The size of aggregation during initial brine and post flush is shown in **Figure 22**. Overall the aggregation size is reduced during brine post flush but some part formed bigger aggregates that possibly occurred when brine keep in contact with nanoparticles blocked in the porous network. Significant aggregates appeared after 1st and 2nd stage of brine injection at specified ROIs (ROI 1, ROI 2, ROI 3, ROI 4, ROI 5 and ROI 6), classified into fine, medium and coarse aggregation size. At initial stage, fine aggregates size during 1st and 2nd brine injection at each ROIs was not significant from one another. Since their size are relatively small, they are found abundantly in suspension mode (unattached to wall) which prone to propagate in the porous network. Medium aggregates size during 1st and 2nd brine injection indicate size reduction from the front (ROI 1/ROI 4) to end (ROI 3/ROI 4). After a week, the aggregates size at each ROIs decreased at about 5% and below. The medium size range during 1st and 2nd brine injection was insignificant which fall between 100 and 170 μm and 60–180 μm. Coarse aggregates size during 1st and 2nd

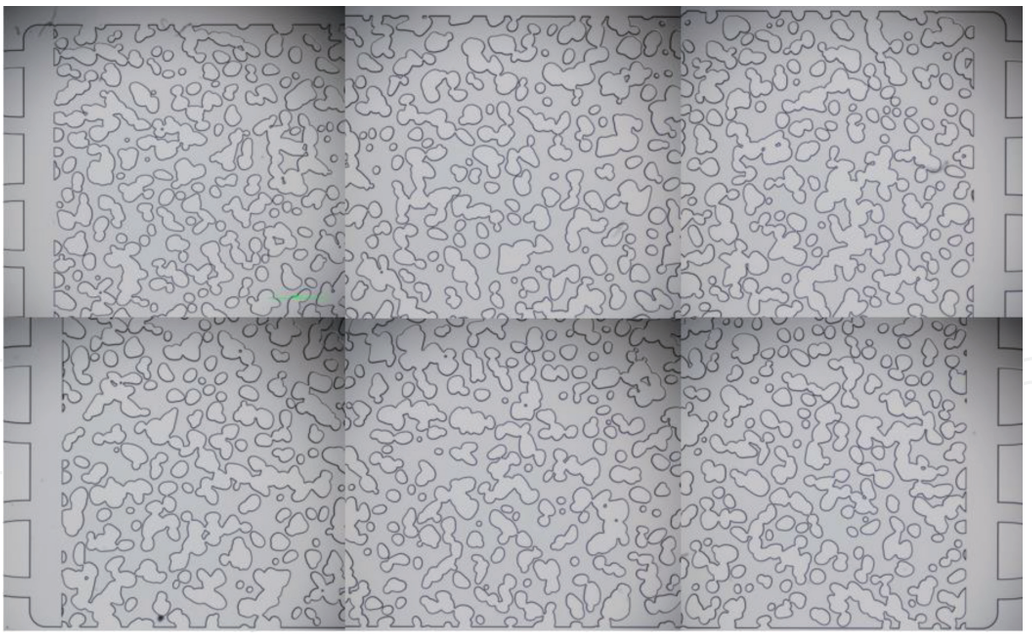

Figure 18.
Micromodel porous network before fluid injection.

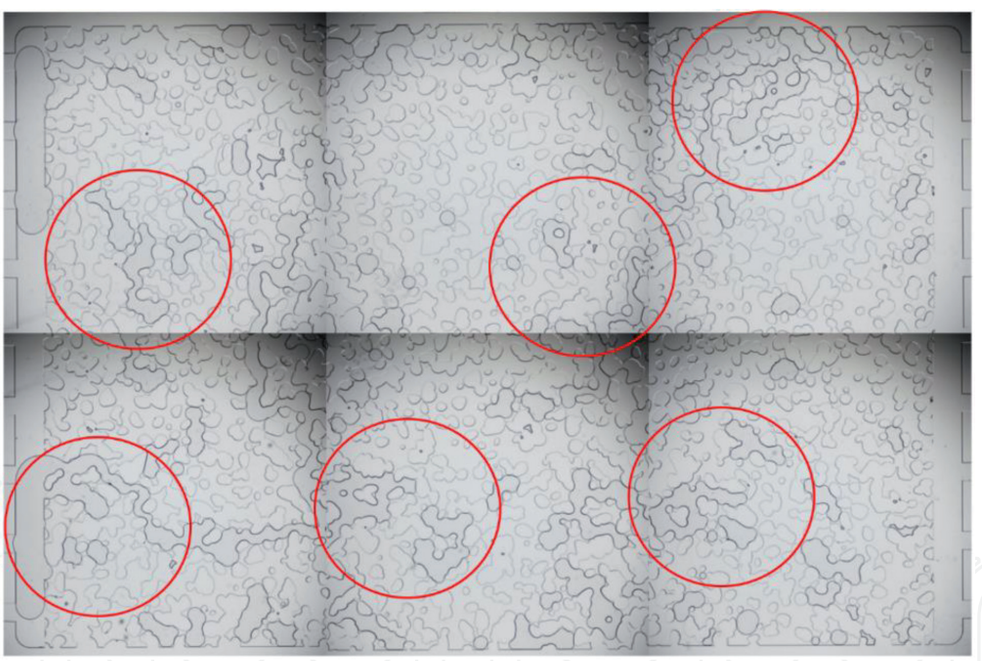

Figure 19.
Micromodel porous network during silica nanoparticles injection. Silica nanoparticles flowed through porous media marked in red circle at ROI 1, ROI 2, ROI 3, ROI 4, ROI 5 and ROI 6.

brine injection indicate size reduction from the front (ROI 1/ ROI 4) to end (ROI 3/ ROI6). After one week aging, the aggregates size decreased at about 10% and below at ROI 3/ROI 5 for 1st brine injection, then decreased at ROI 1, ROI 3 and ROI 5 for 2nd brine injection. The coarse size range during 1st/2nd brine injection are significant which fall between 190 and 340 μm and 160–430 μm.

4. Conclusions

In this study, partially hydrophilic silica nanoparticles adsorption and aggregation in porous media has been demonstrated through quantitative and qualitative

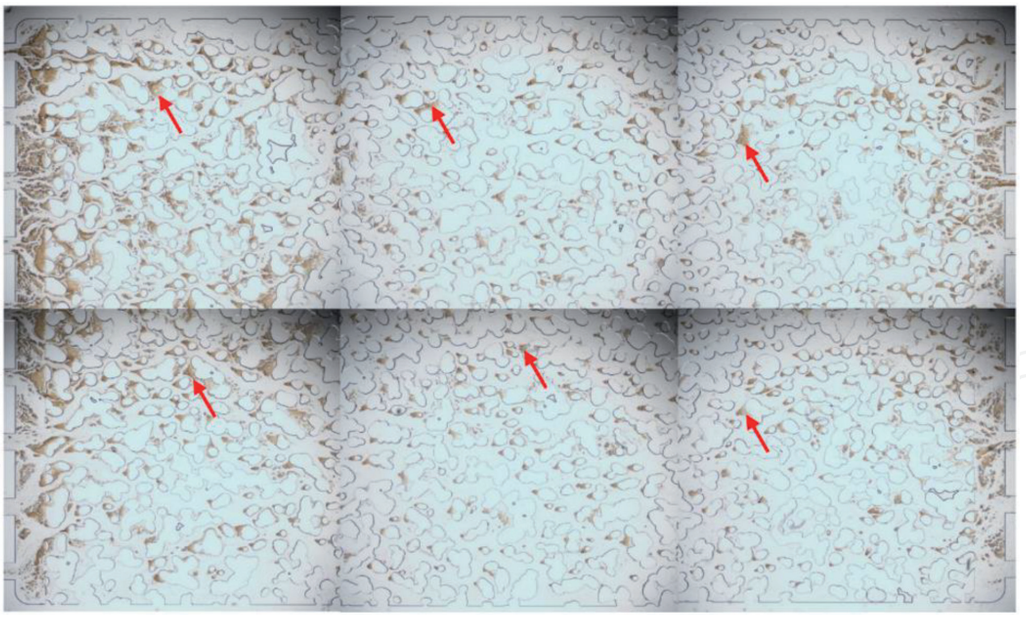

Figure 20.
Micromodel porous network during brine injection and in contact with silica nanoparticles. Gelled-like suspension formed at most of the porous area marked in red arrow.

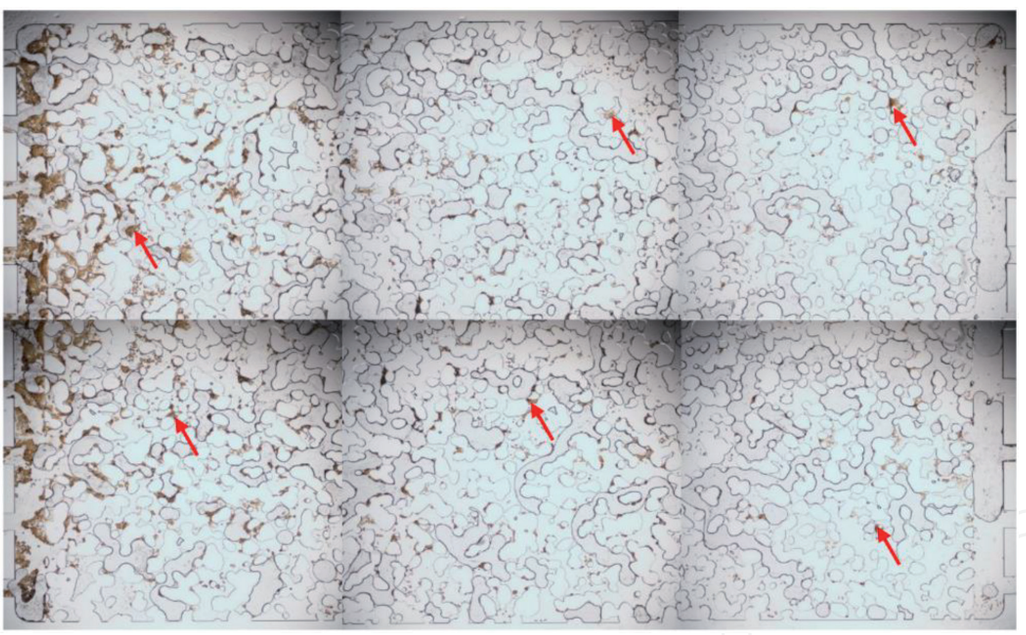

Figure 21.
Micromodel porous network during brine injection (after 1 week ageing). Most of the gelled like suspension pushed out from the porous network. Some adsorbed silica nanoparticles strained inside the porous network.

analysis. Four water wet Buff Berea cores treated with 0.05% silica nanoparticles at 30 and 60°C were evaluated. Micromodel added qualitative information through visualization of silica nanoparticles aggregation in the porous network. The results derived from the experimental work concluded as follows:

- The permeability impairment of treated core at 60°C is slightly lower compared to 30°C. The sharp increase in pressure drops at 60°C during initial silica nanoparticles provided important information of potential log-jamming effect that caused by aggregation of nanoparticles when in contact with water.

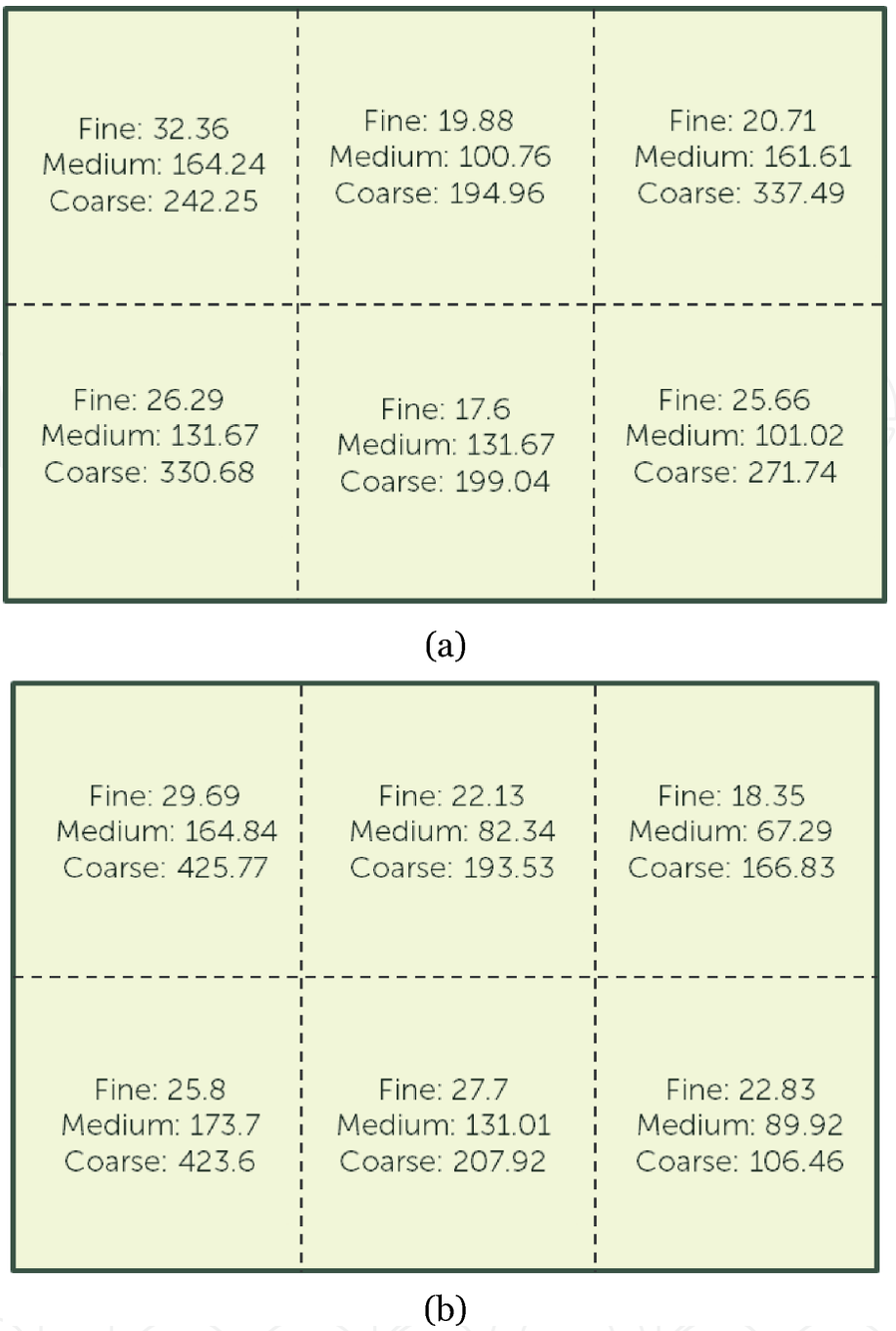

Figure 22.
The average size of silica nanoparticles at fine, medium and coarse classification (a) during initial brine injection (b) brine post flush after 1 week aging.

- From FESEM photomicrographs, most of the silica nanoparticles aggregates observed at the outer section of the treated core that has been pushed out during brine post flush and some remains adsorbed inside the core showed as spherical shape with little aggregates.

- The particles size of core flooding effluents during silica nanoparticles are smaller that supported the high pressure drops value. In contrast, the particles size is much larger during brine post flush supported with low pressure drops value.

- In general, the permeability impairment after silica nanoparticles injection is insignificant and the silica nanoparticles concentration can be further optimized that can be beneficial as improved oil recovery agent with minimum risk of formation damage.

- Micromodel test enable the visualization of silica nanoparticles aggregation in the porous network when in contact with brine. This observation supported the high pressure drops value during core flood when nanoparticles in contact with in-situ brine. Most of the aggregates at coarse section of micromodel network flushed out during brine post flush.

Acknowledgements

The author would like to thank Wan Shah Rizal Abdullah, Ms. Fatin Najihah Jasni, Ms. Nurul Syuhada M Sobri and Mr. Zulkarnain Harom, Ms. Afidah Sastro for their assistance in the laboratory. This research is supported by PETRONAS Research Sdn Bhd and funded by Petroleum Research Fund under cost center E.025.JRD.02017.401.

Conflict of interest

The authors declare no conflict of interest.

Author details

Siti Rohaida Mohd Shafian[1,2*], Ismail M. Saaid[2], Norzafirah Razali[1], Ahmad Fadhil Jahari[2] and Sonny Irawan[3]

1 PETRONAS Research Sdn Bhd, Kajang, Selangor, Malaysia

2 Petroleum Engineering Department, Universiti Teknologi PETRONAS, Tronoh, Perak, Malaysia

3 School of Mining and Geosciences, Nazarbayev University, Kazakhstan

*Address all correspondence to: rohaidashafian@petronas.com.my

References

[1] Ponmani S, Nagarajan R, Sangwai J. Applications of nanotechnology for upstream oil and gas industry. Journal of Nano Research. 2013;**24**:7-15

[2] Negin C, Ali S, Xie Q. Application of nanotechnology for enhancing oil recovery – A review. Petroleum. 2016;**2**(4):324-333

[3] Sun X, Zhang Y, Chen G, Gai Z. Application of nanoparticles in enhanced oil recovery: A critical review of recent progress. Energies. 2017;**10**(3):1-33

[4] Fakoya MF, Pateh H, Shan SN. Nanotechnology: Innovative applications in the oil and gas industry. International Journal of Global Advanced Materials and Nanotechnology. 2018;**1**(1):16-30

[5] Nazari N, Tsau JS, Barati R. CO_2 foam stability improvement using polyelectrolyte complex nanoparticles prepared in produced water. Energies. 2017;**10**(4):1-16

[6] Najafiazar B, Wessel-Berg D, Bergmo PE, Simon CR, Yang J, Torsæter O, et al. Polymer gels made with functionalized organo-silica nanomaterials for conformance control. Energies. 2019;**2**(19):1-25

[7] Lu T, Li Z, Zhou Y. Flow behavior and displacement mechanisms of nanoparticle stabilized foam flooding for enhanced heavy oil recovery. Energies. 2017;**10**(4):1-21

[8] Irfan SA, Shafie A, Yahya N, Zainuddin N. Mathematical modeling and simulation of nanoparticle-assisted enhanced oil recovery – A review. Energies. 2019;**12**(8):1-19

[9] Lau ZY, Lee KC, Soleimani H, Beh HG. Experimental study of electromagnetic-assisted rare-earth doped yttrium iron garnet (YIG) nanofluids on wettability and interfacial tension alteration. Energies. 2019;**12**:1-9

[10] Wang X, Xiao S, Zhang Z, He J. Effect of nanoparticles on spontaneous imbibition of water into ultraconfined reservoir capillary by molecular dynamics simulation. Energies. 2017;**10**(4):1-14

[11] Taborda EA, Franco CA, Alvarado V, Cortes FB. A new model for describing the rheological behavior of heavy and extra heavy crude oils in the presence of nanoparticles. Energies. 2017;**10**(12):1-13

[12] Huang T, Evans BA, Crews JB. Field Case Study on Formation Fines Control with Nanoparticles in Offshore Applications, SPE-13508-MS. Florence, Italy: SPE Annual Technical Conference and Exhibition; 2010

[13] Khan I, Saeed K, Khan I. Nanoparticles: Properties, applications and toxicities. Arabian Journal of Chemistry. 2019;**12**(7):908-931

[14] Agista M, Guo K, Yu Z. A state-of-the-art review of nanoparticles application in petroleum with a focus on enhanced oil recovery. Applied Sciences. 2018;**8**(6):871

[15] Yuan B, Moghanloo RG, Zheng D. Analytical evaluation of nanoparticle application to mitigate fines migration in porous media, SPE-174192-PA. SPE Journal. 2016;**21**(06):2317-2332

[16] Krishnamoorti R. Extracting the benefits for the oil industry. Journal of Petroleum Technology. 2006;**58**:24-26

[17] Zhang T, Murphy M, Yu H, Bagaria HG, Yoon KY, Nielson BM, et al. Investigation of nanoparticles adsorption during transport in porous media. SPE Journal. 2014;**20**:667-677

[18] Yuan B, Wang W, Moghanloo RG, Su Y, Wang K, Jiang M. Permeability reduction of Berea cores owing to nanoparticle adsorption onto the pore surface: Mechanistic modelling and experimental work. Energy & Fuels. 2017;**31**(1):795-804

[19] Abdelfatah E. Multiscale modeling of nanoparticles transport, aggregation and in-situ gelation in porous media [PhD]. Norman, Oklahoma: University of Oklahoma; 2017

[20] Khilar KC, Fogler HS. Migrations of Fines in Porous Media, Xiii. Dordrecht, The Netherlands: Kluwer Academic Publishers; 1998

[21] Agi A, Junin R, Gbadamosi A. Mechanism governing nanoparticle flow behaviour in porous media: Insight for enhanced oil recovery applications. International Nano Letters. 2018;**8**(2):49-77

[22] Giraldo J, Benjumea P, Lopera S, Cortés FB, Ruiz MA. Wettability alteration of sandstone cores by alumina-based Nanofluids. Energy & Fuels. 2013;**27**:3659-3665

[23] Hendraningrat L, Li S, Torsæter O. Effect of Some Parameters Influencing Enhanced Oil Recovery Process Using Silica Nanoparticles: An Experimental Investigation. In: Proceedings of the SPE Reservoir Characterization and Simulation Conference and Exhibition. Abu Dhabi, UAE, Richardson, TX, USA: Society of Petroleum Engineers; 16-18 September 2013

[24] Li S, Torsæter O. The Impact of Adsorption and Transport on Wettability Alteration of Water Wet Berea Sandstone. In: Proceeding of the SPE/IATMI Asia Pacific Oil & Gas Conference and Exhibition. Nusa Dua, Bali, Indonesia, Richardson, TX, USA: Society of Petroleum Engineers; 20-22 October 2015

[25] Erfani Gahrooei HR, Ghazanfari MH. Application of a water based nanofluid for wettability alteration of sandstone reservoir rocks to preferentially gas wetting condition. Journal of Molecular Liquids. 2017;**232**:351-360

[26] DamgaardTS. Experimental investigation of nanoparticle adsorption and pore blockage in intermediate wet berea sandstone [MSc]. Norwegian University of Science and Technology; 2017

[27] Hendraningrat L, Engest B, Suwarno S, Li S, Torsæter O. Laboratory Investigation of Porosity and Permeability in Berea Sandstones Due to Hydrophilic Nanoparticles Retention. In: Proceedings of the International Symposium of the Society of Core Analysts. Napa Velley, California, USA; 16-19 September 2013

[28] Hendraningrat L, Li S, Torsæter O. Improved Oil Recovery by Hydrophilic Silica Nanoparticles Suspension: 2-Phase Flow Experimental Studies. In: Proceedings of the International Petroleum Technology Conference. Beijing, China, Richardson, TX, USA; 26-28 March 2013

[29] Mohd Shafian SR, Jahari AF, Razali N, Irawan S, Ibrahim JM, Salleh IK. Controlling fines migration by enhancing fines attachment using silica nanoparticles. International Journal of Advanced Science and Technology. 2020;**29**(1):318-331